Structural and optical properties of ELOG a-plane GaN grown with MOVPE over different stripe directions on r-plane sapphire

C. Netzel, T. Wernicke, U. Zeimer, and M. Weyers

Ferdinand-Braun-Institut für Höchstfrequenztechnik, 12489 Berlin, Germany

GaN and its alloys with AlN and InN have a strong piezoelectric and spontaneous polarization along the c-axis of the wurzite unit cell. In heterostructures on (0001) c-plane GaN the change in polarization at the interface leads to strong electric fields and a bending of valance and conduction bands [1]. In optoelectronic devices the piezoelectric field over quantum wells results in a reduced oscillator strength and a decrease of the emission energy from the quantum wells (quantum confined Stark effect). Since the polarization vector is parallel to the c-axis, the quantum confined Stark effect can be reduced or avoided by growing GaN in non-c-plane orientation. For nonpolar GaN, e.g. a-plane $(2\bar{1}\bar{1}0)$ or m-plane $(10\bar{1}0)$ oriented layers, the c-axis is perpendicular to the surface and there are no polarization fields over quantum wells, as proven by photoluminescence (PL) [2] and theoretical calculations [3].

a-plane GaN can be grown on r-plane sapphire [4] and a-plane SiC [5]. In both cases the a-plane GaN is very defective. The threading dislocation (TD) density of nonpolar GaN-layers grown by MOVPE is usually $1\text{x}10^{10}$ cm^{-2} [6]. Furthermore, basal plane stacking faults (BSF) are present with a density of $\sim 2\text{x}10^{5}$ cm^{-1}. Additionally to the edge, screw, and mixed type TDs that are also common in c-plane GaN, partial dislocations delimiting BSFs were found [6]. As known from c-plane GaN, epitaxial lateral overgrowth (ELOG) can reduce the threading dislocation density [7]. ELOG with a SiO_2-stripe mask was applied to a-plane GaN [8], too. The growth facets of the overgrown material are determined by the in-plane orientation of the stripe mask [9]. As shown by Haskell et al. [10], a reduction in TD density was observed with stripes parallel [0001], whereas the overgrown regions were free of stacking faults and dislocations with stripes parallel $[10\bar{1}0]$. The aim of our experiments was to study the growth over several stripe directions.

Experimental

The samples were grown using an Aixtron 11x2" multi wafer MOVPE reactor. 1.8 µm thick GaN layers were grown by a two step growth process on 430 µm thick r-plane sapphire substrates. The growth temperature was 1210°C and the growth rate was 2.5 µm/h. These templates were covered with 100 nm sputtered SiO_2. Stripes parallel [0001], $[01\bar{1}1]$ and $[01\bar{1}0]$ were patterned with a mask window of 5 µm and a period of 15 µm. After stripe definition the wafers were overgrown for 2 hours at 1270°C.

The samples were investigated using scanning electron microscope (SEM), cathodoluminescence (CL), and photoluminescence (PL). For cross sectional investigation, the samples were scribed and broken perpendicular to the ELOG stripe pattern.

SEM results

In fig. 1 cross sectional SEM micrographs of the three kinds of stripe orientations are shown. Depending on the stripe orientation, different growth facets and therefore different growth rates can be observed. Fig. 1a shows a cleaved edge of the sample with stripes parallel [0001], where the top facet parallel to the substrate surface is a $(2\bar{1}\bar{1}0)$ plane. The other facets perpendicular and inclined to the surface are $\{10\bar{1}0\}$ planes. Since the side wall facets are equivalent in sense of crystal symmetry, the overgrowth is symmetric. The lateral growth rate is 1.5 µm/h and the vertical growth rate is 3.8 µm/h. The width of the top facet decreases during growth from 5 µm to 2.5 µm. This facet grows faster than $\{10\bar{1}0\}$ facets and would vanish during subsequent growth.

For stripes parallel $[01\bar{1}1]$ a $(2\bar{1}\bar{1}0)$ top facet is observed as well (fig. 1b). The width of this facet is increased during growth. The inclined facet on the left hand side of the stripe is a N-polar $(10\bar{1}\bar{1})$-facet, whereas the inclined facet on the right is a Ga-polar $(1\bar{1}01)$-facet. The facet perpendicular to the surface is $(0\bar{1}12)$. The growth is very asymmetric. The Ga-polar facets have a much larger lateral growth rate of 4.4 µm/h compared to the $(10\bar{1}\bar{1})$ facet with a lateral growth rate of 1.1 µm/h. Due to this asymmetry the $(2\bar{1}\bar{1}0)$-facet is not vertically aligned to the win-

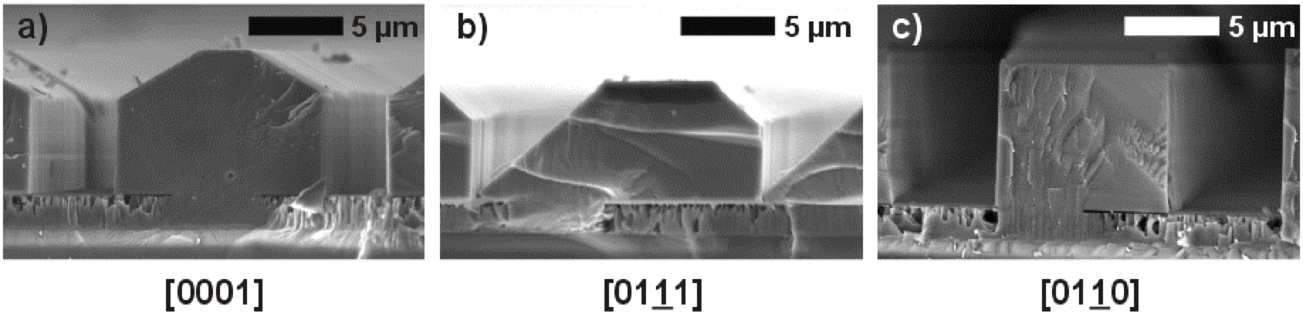

Fig. 1 Scanning electron micrographs of the cross sections of ELOG stripes with stripe orientation parallel to a) [0001], b) [01$\underline{1}$1], and c) [01$\underline{1}$0].

dow of the mask. The higher lateral growth rate of the Ga-face results in a faster coalescence. The vertical growth rate is 3 µm/h.

For the sample with stripes parallel [01$\underline{1}$0] in fig. 1c the profile is rectangular like described by *Craven et al.* [9]. The top facet is (2$\underline{1}\underline{1}$0) again and the side facets are (000$\underline{1}$) and (0001) on the left and on the right hand side of the stripe, respectively [11]. Similar to the [01$\underline{1}$1] stripe orientation the Ga-polar facet grows much faster (2.2 µm/h) than the N-polar facet (0.1 µm/h). The width of the top facet grows with a rate of 2.2 µm/h, too. The vertical growth rate of these stripes is 3.8 µm/h. Due to the completely different growing facets causing another growth rate and surface chemistry, a different defect incorporation and threading dislocation propagation can be expected.

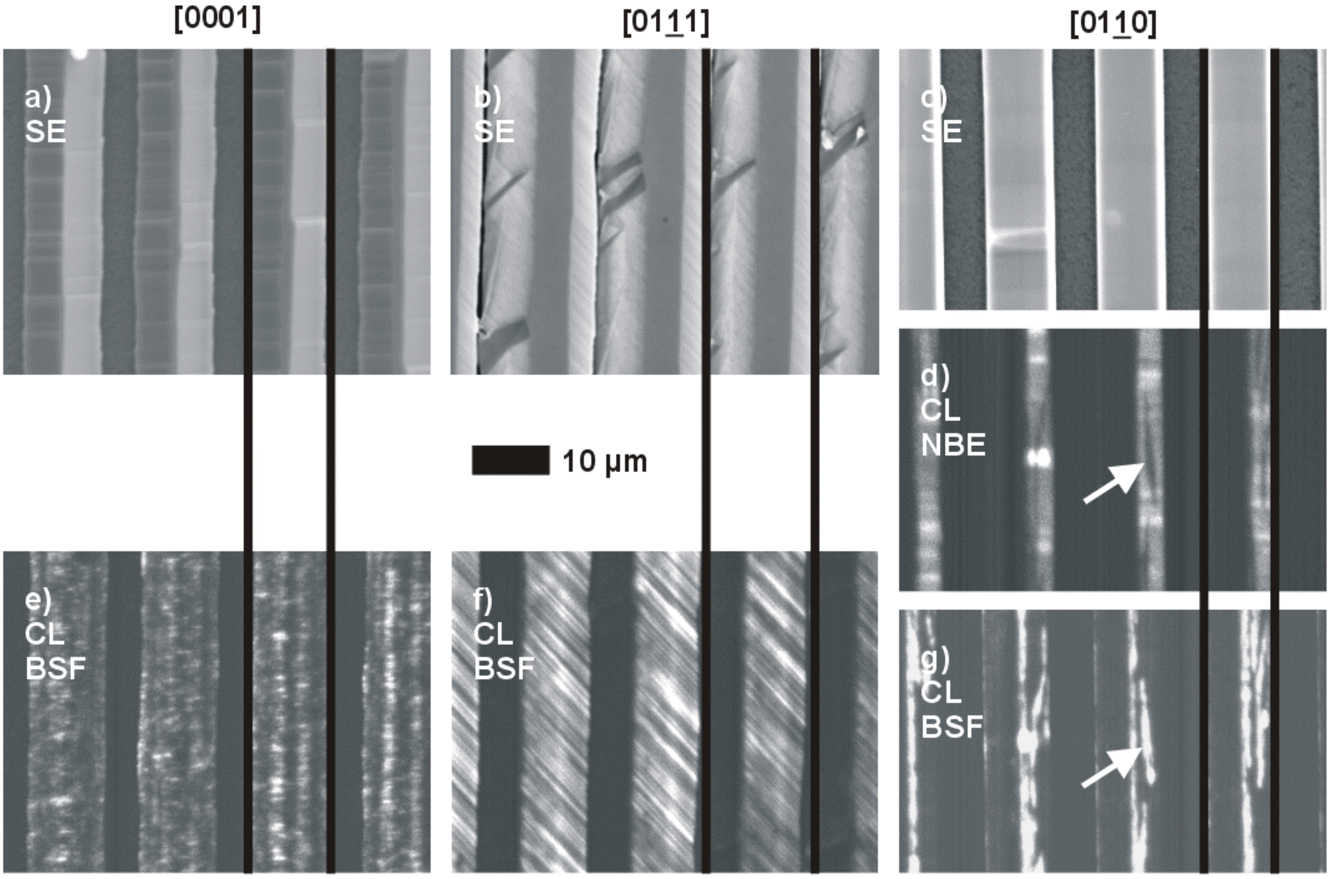

Fig. 2 (a) – (c) plan view secondary electron micrographs of samples with [0001], [01$\underline{1}$1] and [01$\underline{1}$0] stripes; (d) – (g) monochromatic CL micrographs of the same area as above: (d) NBE at 3.463 eV or 358 nm, (e) – (g) BSF peak position at about 3.415 eV or 363 nm. One stripe of each sample is marked by black lines to show the alignment of the images.

Cathodoluminescence results

Spectrally and laterally resolved cathodoluminescence (CL) investigations were carried out at 80 K in a conventional SEM in plan-view geometry. Since the overgrown layer thickness of the samples is larger than 5 µm an acceleration voltage of 20 kV was used to penetrate at least 1 µm into the sample. Thus, the information depth covers only the near surface regions of the overgrown layer. Monochromatic CL micrographs are collected at the main peaks arising in the integrated spectrum for each sample which was taken over an area of 57 x 47 µm^2 (fig. 2a – g).

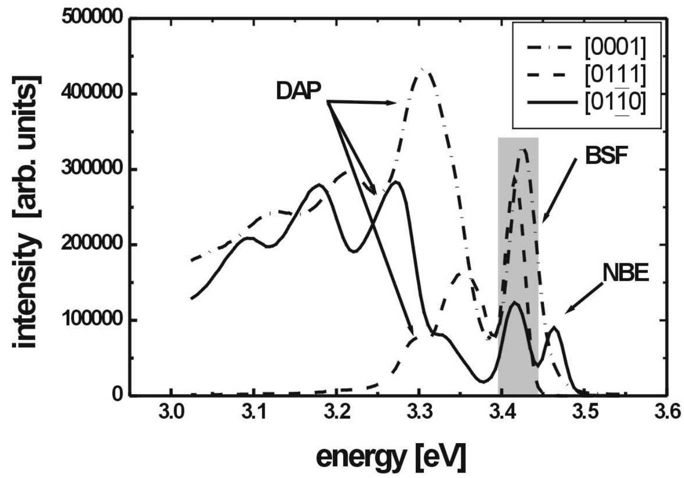

Fig. 3 80 K CL spectra integrated over an area of 57 x 47 µm^2

The spectra are shown in fig. 3. At 80 K only for the sample with stripes parallel to [01$\underline{1}$0] the near bandedge emission (NBE) luminescence was observed. However, as for the sample with [0001] stripes the highest intensity peaks arise from the donor-acceptor pair (DAP) transitions. The samples with stripes parallel to [01$\underline{1}$1] and [0001] show a high intensity peak at 3.415 eV (see grey area in fig. 3) which is attributed to the BSF luminescence indicating a high number of BSFs in these samples. As already pointed out by Liu et al. [12], a high number of stacking faults suppresses the NBE emission.

Generally, the luminescence intensity in the wing regions is much higher than in the window regions. In fig. 2 monochromatic images taken at the BSF luminescence peak at 3.415 eV are shown for all samples as well as the monochromatic image at the NBE peak for the sample with stripes parallel [01$\underline{1}$0]. In case of the symmetric growth over the [0001] stripe (fig. 2e) the intensity distribution of the BSF luminescence is symmetric. For [01$\underline{1}$1] stripes the window region (fig. 2f, region indicated by an arrow) shows almost no luminescence (see also fig. 1b, left hand side of the stripe). This is due to a high nonradiative recombination in this region that is caused by a high TD density. The direction of the stacking fault plane is inclined by 45° or perpendicular to the stripe direction, respectively, as seen in figs. 2f and e. Bright lines or dots align along these directions. The density of the bright lines is $2x10^4$ cm^{-1}. This is smaller than the BSF density reported in literature. It can be assumed, that no single BSF were resolved, but bunches of BSF. The window regions appear also dark for the sample with stripes parallel to [01$\underline{1}$0] (see fig. 2d and g). The number of BSFs is clearly reduced in the wing region compared to the other samples. Note the anticorrelation of intensity in both images (arrow in fig. 2d and g) which also indicates the suppression of NBE luminescence by BSFs that appear as dark lines along the stripe in fig. 2d.

Photoluminescence results

For the PL measurements an excitation power density of about 1 W/cm^2 from a HeCd-laser with λ = 326 nm was used. The sample temperature was varied between 10 K and 250 K. Temperature dependent PL from the three wafers with [0001]-, [01$\underline{1}$1]-, and [01$\underline{1}$0]-stripes was measured with a macroscopic excitation spot of about 400 µm in diameter. The PL signal is integrated over the different facets of the ELOG stripes in these experiments.

In fig. 4 the temperature dependence of the PL emission from the sample with stripes parallel to [01$\underline{1}$0] is displayed. The PL spectra for four temperatures and the decrease of the integrated intensity of each emission (yellow luminescence, DAP, BSF, and NBE) are shown. As observed in the CL, in PL measurements too, we observe strongest NBE emission from the ELOG structure with stripes parallel to [01$\underline{1}$0]. At T = 10 K the NBE emission dominates the emission spectra. A reduction of competing radiative and nonradiative processes can be assumed for this structure. The temperature dependence for all samples with varying stripe orientations are similar. The intensity starts to decrease already at 10 K for all emissions. This shows the high influence of the nonradiative recombination processes even at lowest temperatures.

The intensity decrease below 100 K is most distinct for the NBE emission and the stacking faults. The intensity decreases to less than 5 % in this temperature range. Charged carriers are hardly hindered to recombine nonradiatively in the ELOG GaN structures. Even carriers in the quantum well like potential valley of the BSFs obviously do not reveal an increased suppression of nonradiative recombination when compared with the NBE emission. The temperature dependent integrated intensity decreases almost alike.

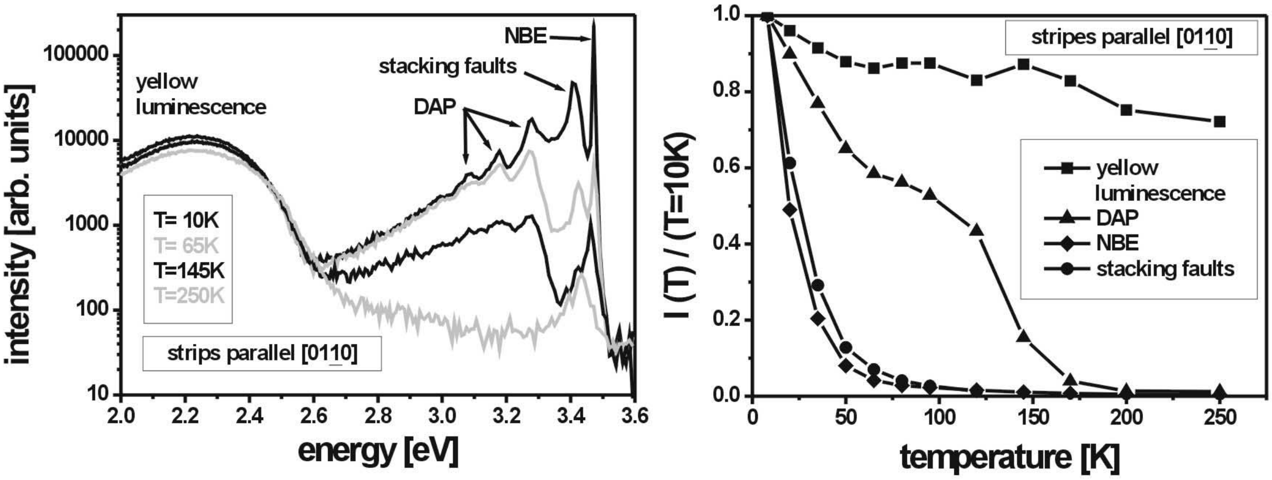

Fig. 4 Temperature dependent PL from the ELOG GaN structure with stripes parallel [01$\bar{1}$0].

Summary

The growth of ELOG GaN on patterned a-plane GaN has been studied. Several growth facets are formed during the overgrowth step. The CL and PL studies point to best results for reduced nonradiative recombination and reduced defect density in a-plane ELOG GaN with stripes parallel to [01$\bar{1}$0]. Temperature dependent PL shows the high influence of nonradiative recombination even at lowest temperatures. No significant difference in the temperature dependent intensity decrease is present among the samples with varying ELOG stripe directions.

Acknowledgements

The authors would like to thank F. Brunner and T. Petzke for supervising the MOVPE growth and H. Lawrenz for performing PL measurements.

References

[1] S. H. Park, J. Appl. Phys., **91**, (2002), 9904-9908.
[2] M. D. Craven, P. Walterit, J. S. Speck ,and S. P. DenBaars, Appl. Phys. Lett., **84**, (2003), 496-498.
[3] T. Takeuchi, H. Amano, and I. Akasaki, Jpn. J. Appl. Phys., **39**, (2000), 413-417.
[4] M. Sano ,and M. Aoki, Jpn. J. Appl. Phys., **15**, (1976), 1943-1949.
[5] M. D. Craven, F. Wu, A. Chakraborty, B. Imer, U. K. Mishra, S. P. DenBaars, and J. S. Speck, Appl. Phys. Lett., **84**, (2004), 1281-1283.
[6] M. D. Craven, S. H. Lim, F. Wu, J. S. Speck ,and S. P. DenBaars, J. Appl. Phys., **81**, (2002), 469-471.
[7] B. Beaumont, Ph. Vennéguès, and P. Gibart, Phys. Stat. Sol. (b), **227**, (2001), 1–43.
[8] C. Chen, J. Yang, H. Wang, J. Zhang, V. Adivarahan, M. Gaevski, E. Kuokstis, Z. Gong, M. Su, and M. A. Kahn, Jpn. J. Appl. Phys., **42**, (2003), L640-L642.
[9] M. D. Craven, S. H. Lim, F. Wu, J. S. Speck ,and S. P. DenBaars, Appl. Phys. Lett., **81**, (2002), 1201-1203.
[10] B. A. Haskell, F. Wu, M. D. Craven, P. T. Fini, T. Fuji, K. Fujito, S. P. DenBaars, J. S. Speck, and S. Nakamura, Appl. Phys. Lett., **83**, (2003), 644-646.
[11] F. Wu, M. D. Craven, S. H. Lim, and J. S. Speck, J. Appl. Phys., **94**, (2003), 942.
[12] R. Liu, A. Bell, F. A. Ponce, C. Q. Chen, J. W. Wang, and M. A. Khan, Appl. Phys. Lett., **86**, (2005), 021908.